Journal of Zhejiang University-SCIENCE A (Applied Physics & Engineering) 2025 26(2):166-176
www.jzus.zju.edu.cn; www.springer.com/journal/11582
E-mail: jzus_a@zju.edu.cn

Research Article

https://doi.org/10.1631/jzus.A2300645

A molecular dynamics simulation study on the tensile and compressive behavior of hydrated kaolinite

Ming LU[1,2], Qiufeng DIAO[1,2], Yuanyuan ZHENG[1,2]✉

[1]*School of Civil Engineering, Sun Yat-Sen University, Guangzhou 510275, China*
[2]*Southern Marine Science and Engineering Guangdong Laboratory (Zhuhai), Zhuhai 519082, China*

Abstract: Clay minerals can experience strong tensile and compressive forces in extreme environments such as the deep sea and subsurface. Moreover, the presence of water films greatly affects the mechanical properties of clay. To explore these properties, we use a molecular dynamics (MD) simulation method to study axial mechanical behavior and failure mechanisms of hydrated kaolinite. Two types of deformation are applied to kaolinite examples with varying water film thicknesses: stretching along the transverse (x) direction, and compression along the longitudinal (z) direction. The ultimate strengths of hydrated kaolinite with different water film thicknesses range from 8.12% to 27.53% (for stretching along the x-direction) and from 15.71% to 26.02% (for compression along the z-direction) less than those of dehydrated kaolinite. Additionally, we find that hydrated kaolinite is more prone to tensile than compressive failure under high stress. When stretched along the x-direction, the diffusion of water molecules results in unstable tensile properties. When compressed along the z-direction, water films weaken the compressive strength of the system and lead to greater compressive deformation, but also delay the time at which the system fails. Furthermore, we investigated the failure mechanisms of hydrated kaolinite through analysis of interaction energies. The tensile failure along the x-direction is caused by the breaking of the covalent bonds in the clay mineral sheet. On the other hand, the compressive failure along the z-direction is due to the crushing of the internal structure of the clay mineral sheet.

Key words: Kaolinite; Uniaxial strain; Molecular dynamics (MD); Water film

1 Introduction

Settlement consolidation, tunnel excavation, and oil and gas production are often performed in extreme environments like the deep ocean or subsurface (González et al., 2012; Wongsaroj et al., 2013). Hydrated clays, as part of rocks in these environments, are subjected to high stresses (Zhang, 2018). The mechanical properties of clay can be weakened by water, which may lead to microscopic damage under high tension and compression, and cause serious engineering hazards (Milheiro et al., 2005; Zhao et al., 2007). However, knowledge of the micro-mechanics that govern the structural changes of hydrated clay is still limited. Kaolinite is a common non-swelling clay mineral, which can absorb water molecules to form water films, thereby influencing the macroscopic mechanical properties (Tunega et al., 2004; Šolc et al., 2011; Lu et al., 2025). Therefore, it is crucial to investigate the mechanical behavior and failure mechanisms of hydrated kaolinite under high tension and compression.

Macroscopic experiments have demonstrated that water films have a significant impact on the mechanical properties of clay, such as limiting the water content (Moreno-Maroto and Alonso-Azcárate, 2015; Spagnoli et al., 2017). The reason for this phenomenon is that the clay gradually forms different bound water films as the water content increases (Ma et al., 2019). However, there is little research on hydrated kaolinite under high stress, especially investigating the mechanisms at the microscopic level.

Molecular dynamics (MD) enables the study of the physical properties of micro-clay minerals at the atomic scale, which leads to an improved understanding of the deformation and failure mechanisms of such materials (Fan et al., 2023). The MD simulation method has

✉ Yuanyuan ZHENG, zhengyy57@mail.sysu.edu.cn
Ming LU, https://orcid.org/0000-0001-8723-590X
Yuanyuan ZHENG, https://orcid.org/0000-0002-5076-213X

Received Dec. 23, 2023; Revision accepted Apr. 15, 2024; Crosschecked Jan. 22, 2025

been employed to study the mechanical behaviors of dehydrated kaolinite; for example, in the elastic–plastic stretching of kaolinite, the most broken bond in the atomic structure at all stages is the Al–O bond (Yang et al., 2019). It has been found that the weakest mechanical properties of clay minerals are attributed to networks of hydrogen bonds (Duque-Redondo et al., 2014). The surface energy of the clay has also been exploited in some studies (Benco et al., 2001) to investigate the failure mechanism of kaolinite. Zhang et al. (2021) simulated the uniaxial strain behavior of dehydrated kaolinite and obtained its anisotropic mechanical response.

However, with regard to the influence of water on kaolinite, most MD simulations have only studied the anisotropic adsorption (Smirnov and Bougeard, 1999; Liu et al., 2012) and diffusion behavior (Chen et al., 2019; Sun et al., 2021; Lu et al., 2024c) of water molecules. Research on the mechanical properties of nanoscale clay minerals with water films has mostly focused on montmorillonite (Wei et al., 2023), illite (Lu et al., 2024b), but not kaolinite. However, the short- and long-term reliability and failure properties of clay (e.g., cracks during tension and collapse during compression) are vital for various engineering applications (Armand et al., 2013). Furthermore, the presence of interlayer water films makes clay minerals highly susceptible to damage during tension and compression. Therefore, it is important to investigate the mechanism by which water films weaken the tensile/compressive properties of hydrated kaolinite.

Accordingly, we investigate the influence of water films on the tensile and compressive properties of kaolinite using the MD simulation method. Uniaxial tension along the transverse (x) direction and uniaxial compression along the longitudinal (z) direction were applied on kaolinite having one to four layers of interparticle water molecules. The deformation and failure mechanisms of these different kinds of hydrated kaolinite are then studied.

2 Simulation methods

2.1 Modeling

Kaolinite is a 1:1 clay mineral composed of one octahedral alumina sheet and one tetrahedral silica sheet, having the unit-cell formula of $Al_2Si_2O_5(OH)_4$, as illustrated in Fig. 1c. The atomic structure of kaolinite was elucidated using X-ray diffraction measurements with

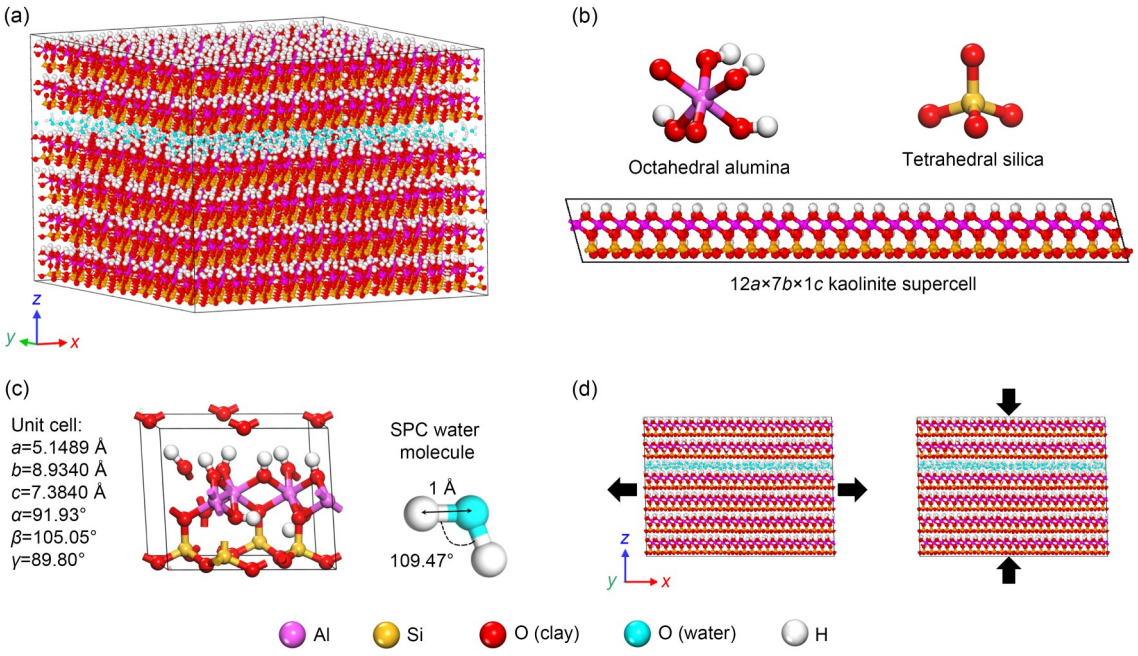

Fig. 1 Simulation details of the model: (a) kaolinite with one water film layer; (b) 12a×7b×1c kaolinite supercell and two kinds of polyhedron sheet; (c) kaolinite crystal and SPC water molecule; (d) uniform tensile deformation along the x-direction and compressive deformation along the z-direction. The tensile and compressive strain rates of deformation were 1×10^{-6} fs^{-1}. The atoms are colored according to their types. References to color refer to the online version of this figure

the unit-cell parameters a=5.1489 Å, b=8.9340 Å, c=7.3840 Å, α=91.93°, β=105.05°, and γ=89.80° (Neder et al., 1999). The simple point charge (SPC) water model was applied in this clay–water system, with a bond length of 1 Å and an angle of 109.47° (Jorgensen et al., 1983). As shown in Fig. 1a, the clay mineral sheet is the 12a×7b×6c kaolinite supercell formed by replicating the unit cell. This size is large enough to ignore size effects on mechanical simulations. In addition, 420, 840, 1260, and 1680 water molecules are added between the particles of kaolinite to form one to four layers of water films, respectively (Lu et al., 2024a).

2.2 Simulation details

The simulations were performed using LAMMPS (Largescale Atomic/Molecular Massively Parallel Simulator) (Plimpton, 1995). Furthermore, we used the ClayFF force field (Cygan et al., 2004), which is a popular function for simulating the crystal structure of clays (Porion et al., 2007; Suter et al., 2007) and the mobility of interlayer water (Leng and Cummings, 2006; Kalinichev et al., 2007). As a general-purpose force field for molecular simulations of layered materials and their fluid interfaces, ClayFF primarily incorporates non-bonded potentials, where only hydroxyls and water molecules incorporate bond stretching and bond-angle bending terms. This ensures the accuracy of predictions while simplifying calculations (Tang et al., 2019; Geng et al., 2024). Other studies have shown that physical properties are accurately reproduced in similar simulations, including energy properties such as elastic constants, bulk modulus, dielectric constants, vibrational spectra, and stress–strain relations (Pouvreau et al., 2019; Tararushkin et al., 2022).

The Coulombic interactions, van der Waals interactions, bond stretching, and angle bending are expressed in Eqs. (S1)–(S6) of the electronic supplementary materials (ESM). Periodic boundary conditions are applied in all directions, allowing particles to interact across the boundaries, exit at one end of the box, and re-enter at the other end. Both the temperature (T) and pressure (P) were controlled using the Nosé-Hoover schemes (Hoover, 1985). The cutoff of the van der Waals force was set at 10 Å. Long-range Coulombic interactions were computed using the Ewald summation with a tolerance of 1×10^{-4}. The system was brought through a two-step process under standard ambient conditions (T=300 K; P=101325 Pa) using the NPT (constant-pressure, constant-temperature) ensemble. First, a 500-ps-long simulation was performed and the system reached a steady state after this equilibrium process. Next, we simulated the tensile and compressive deformations at 500 ps.

It is well-established that the longitudinal compression of clay will invariably result in transverse tension given unconfined conditions; the inverse holds as well. Considering this phenomenon, we implement two custom uniform deformations on kaolinite with varying water film thicknesses. Specifically, uniform tensile and compressive deformations are applied along the x-direction (1 0 0) and z-direction (0 0 1), respectively, with a strain rate of 1×10^{-6} fs^{-1}, as depicted in Figs. 1c and 1d. During the process of tension and compression, data sampling was performed every 1 ps.

3 Results and discussion

3.1 Stress

Fig. 2a shows the stress–strain curves under stretching along the x-direction, and the tensile strength and strain at failure (or ultimate tensile strength and strain) at the failure point F_x are shown in Table S1 of the ESM. As expected, the tensile stress on the systems decreases with the increase in the water film thickness. The failure tensile strengths (or ultimate tensile strengths, point F_x) of hydrated kaolinite range from 8.12% to 27.53% less than those of dehydrated kaolinite. However, the corresponding failure strain (or ultimate tensile strain, point F_x) is very similar (ε_x=0.13). Hence, the water film weakens the tensile strength of hydrated kaolinite but does not affect the critical condition for its failure.

The atomic bond length can be analyzed using a radial distribution function (RDF) (Fan et al., 2022; Zhang and Song, 2022), which represents the probability of the central atom finding the target atom. The coordination number is obtained by integrating the radial distribution function. In Fig. S1 of the ESM, the coordination number corresponding to the first trough of the RDF curve represents the number of atoms bonded to the central atom (Zhang et al., 2014). St, Ao, Ob, and Oh represent the tetrahedral silicon, octahedron aluminum, bridge oxygen, and hydroxyl oxygen, respectively. For example, in the Ao–Oh curve in Fig. S1a, each Ao atom is connected to four Oh atoms, with a bond length of r=2.99 Å. Therefore, we formed virtual Ao–Oh,

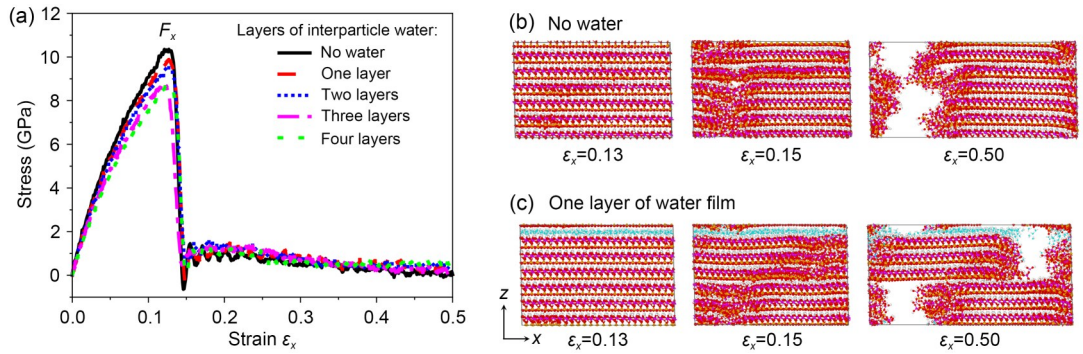

Fig. 2 Mechanical response of dehydrated and hydrated kaolinite when stretched along the *x*-direction: the stress–strain curves (a); the snapshots in the tensile process of dry (b) and hydrated (c) kaolinite. Point F_x is defined as the moment of structural failure. The hydrated kaolinite in Fig. 2c is the case with one layer of water film. References to color refer to the online version of this figure

Ao–Ob, and St–Ob bonds in kaolinite with the distances of 2.99 Å, 3.20 Å, and 2.06 Å, respectively, as shown in Figs. S1a–S1c. Based on this, the relationship between the bonds and the deformation and failure can be studied, as shown in the snapshot images of Figs. 2b and 2c. It can be seen that when ε_x=0.13, the tensile failure was mainly caused by the breaking of covalent bonds in the clay mineral sheet. Moreover, when ε_x=0.50, the clay mineral sheet was split into two parts.

Fig. 3a shows the stress–strain curve resulting from compression along the *z*-direction, with negative values representing compressive stress. It is clear that the water films have a significant effect on the longitudinal compressibility of kaolinite. The failure compressive strengths of hydrated kaolinite range from 15.71% to 26.02% less than those of dehydrated kaolinite (Table S1). Furthermore, the failure compressive strain increases as the number of layers of water film increases, meaning that the water films act to delay the failure time of kaolinite. It can be seen in Figs. 3b and 3c that the clay mineral sheet and water film were slightly disturbed at failure point F_z, and subsequently at failure strain ε_z= 0.27, the structures were completely crushed.

Overall, the compressive strength is much higher than the tensile strength, although it is weakened more significantly by water (Table S1). The van der Waals force can be used to explain the higher stress levels (Eq. (S2) and Fig. S2), since atoms need to overcome these attractions for stretching behavior to occur. The van der Waals force between particles will first increase and then gradually decrease as distance increases, indicating that the stretching between two atoms becomes easier. Conversely, the van der Waals forces cause repulsion when the atoms are compressed, which increases significantly as the atomic spacing becomes closer. The same is true for Coulombic potential energy (Eq. (S1)). Hence, the compressive stress is higher than the tensile stress, and overall, the tensile strengths of dehydrated and hydrated kaolinite are both far lower than their compressive strengths (Table S1). Therefore, kaolinite

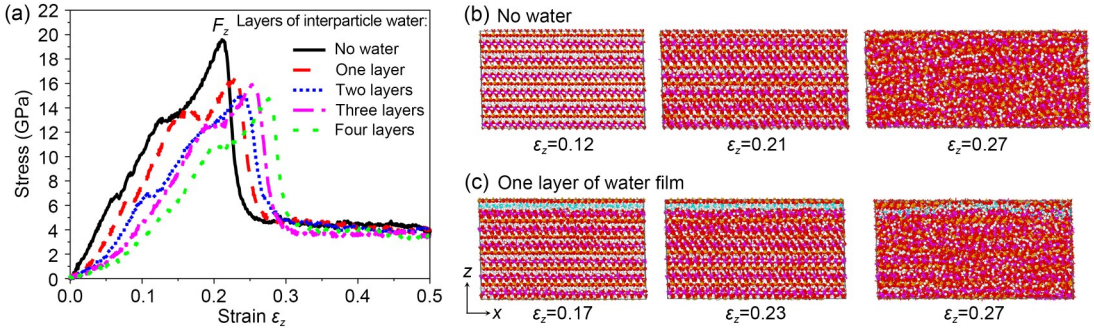

Fig. 3 Mechanical response of dehydrated and hydrated kaolinite compressed along the *z*-direction: the stress–strain curves (a); snapshots during the compressive process of dry (b) and hydrated (c) kaolinite. Point F_z is defined as the moment of structural failure. The hydrated kaolinite in Fig. 3c is the case with one layer of water film. References to color refer to the online version of this figure

mineral sheets in extreme environments are more susceptible to tensile failure than compressive failure.

Hydrated kaolinite systems can be divided into two components to analyze the weakening mechanism of water films: clay mineral sheets and water films. The stresses on each component were calculated separately, as shown in Fig. 4. When stretching along the *x*-direction (Fig. 4a), the trends for the hydrated kaolinite are very similar to that of the dehydrated kaolinite for the stress of the clay mineral sheet. In fact, both the failure stresses and strains (at point F_x) are almost equal for dehydrated and hydrated kaolinite. Thus, the tensile properties of kaolinite mineral sheets are not affected by water films when kaolinite is subjected to uniform stretching along the *x*-direction.

However, for differing water film thicknesses, the stress curves are not as similar, as shown in Fig. 4b. The unstable diffusion of water molecules results in significant stress fluctuations on the water film, even reaching negative values (which correspond to compressive stresses). The average stresses for one to four layers of water films before failure (before the dashed line at ε_x= 0.13) were calculated, and were 0.051, −0.0012, −0.014, and −0.0086 GPa, respectively. The stress on the water film decreases as its thickness increases, and the stress on a single water film layer is much more significant. Therefore, Fig. 2a shows that the kaolinite with one water film layer is subjected to higher tensile stress, while the lower stresses of other water films make that of the other cases lower. In conclusion, the thicker the water film, the smaller the stress on it, which leads to a smaller tensile stress on the clay–water system. This is the basic mechanism by which water films weaken the tensile properties of kaolinite.

The trend of the stress–strain curve when hydrated kaolinite was compressed along the *z*-direction is entirely different from that of the tensile curve. The curves in Figs. 4c and 4d almost coincide with the curves of the clay–water system in Fig. 3a, which means that the strength and development of compressive stress in the clay mineral sheets and the water films are similar. This is because the water films and clay mineral sheets repelled each other during the compression process, and the stress at the contact surface is the same (Fig. S3 of the ESM).

In the compression process, the water film weakens the compressive properties of hydrated kaolinite for two reasons. First, the water film increases the volume

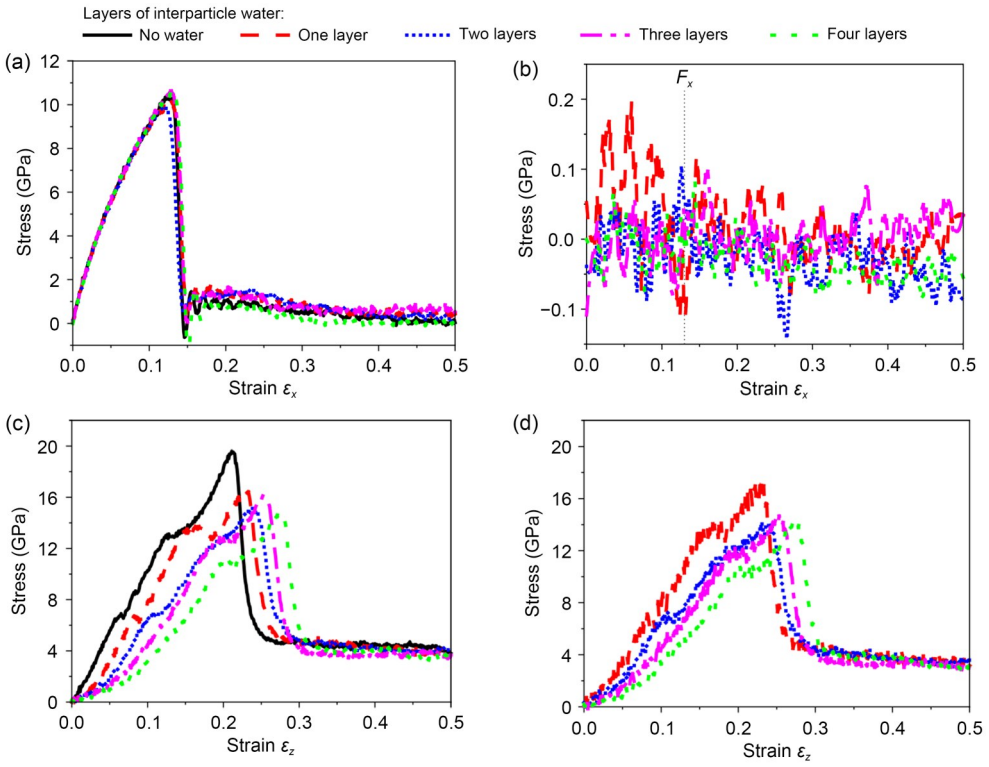

Fig. 4 Stress–strain curves of the clay mineral sheet (a) and water film (b) when stretched along the *x*-direction, and those of the clay mineral sheet (c) and water film (d) when compressed along the *z*-direction

of the clay–water system, so the stress as a volumetric force decreases with the thickening of the water film. Second, the water film divides the clay mineral into two parts. As the thickness of the water film increases, compressing the two adjacent mineral sheets becomes more difficult.

3.2 Strain

3.2.1 Strain stretching along the *x*-direction

The volumetric strain (ε_v) and linear strain (ε_z) of the system during stretching along the *x*-direction can be observed. Fig. 5a shows that the system's volume increases under uniform stretching, and the volumetric strain (ε_v) decreases with an increase in the water film thickness. As shown in Fig. 5b, compression occurs along the *z*-direction with stretching, and the linear strain (ε_z) decreases more significantly as the water film thickens because of the high compressibility of the water film. Hence, interparticle water films can promote compression along the longitudinal direction, thereby delaying volumetric expansion (Fig. 5a).

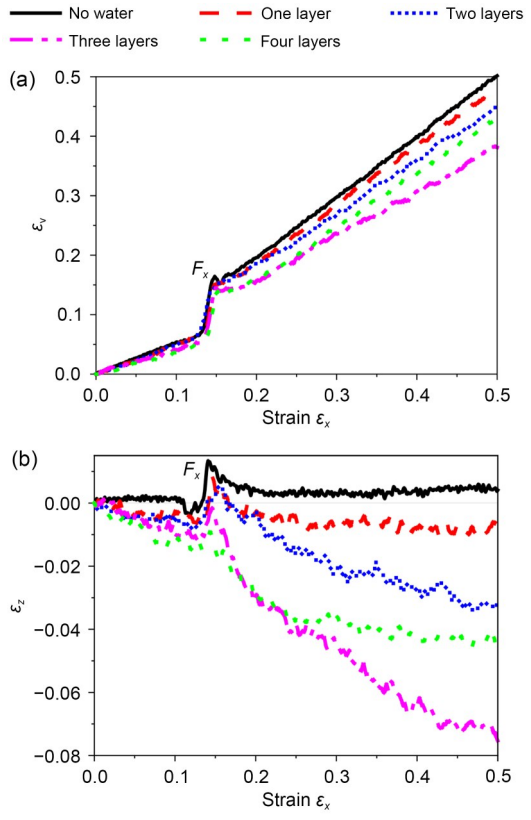

Fig. 5 Strains of dehydrated and hydrated kaolinite when stretching along the *x*-direction: (a) volume strain ε_v; (b) linear strain ε_z

In addition, it can be seen in Fig. 4 that the failure strains (at point F_x) are similar for all cases. As mentioned earlier, the water film thickness does not affect the tensile properties of the clay mineral sheet, nor does it change the system's length (l_x, the initial length $l_{x0}\approx$ 62.25 Å). The tensile values (Δl_x) were similar under the same strain ε_x. Hence, all five clay cases will be destroyed when the covalent bond breaking point ($\Delta l_x = \varepsilon_x \cdot l_{x0} \approx 8.09$ Å, where the failure strain is $\varepsilon_x = 0.13$) is reached. Broken covalent bonds in the clay mineral sheets are the reason for failure when stretching along the *x*-direction.

3.2.2 Compression along the *z*-direction

Two volumetric strain curves were obtained when all cases were compressed along the *z*-direction. Fig. 6a shows the volumetric strain of the clay–water system, and Fig. 6b shows the volumetric strain for the clay mineral sheets themselves. As shown in Fig. 6a, the failure volumetric strain ε_v (at point F_z) of the system decreases as the water film thickness increases. The thicker the water film, the more compressible the system. However, in Fig. 6b, the failure volumetric strains

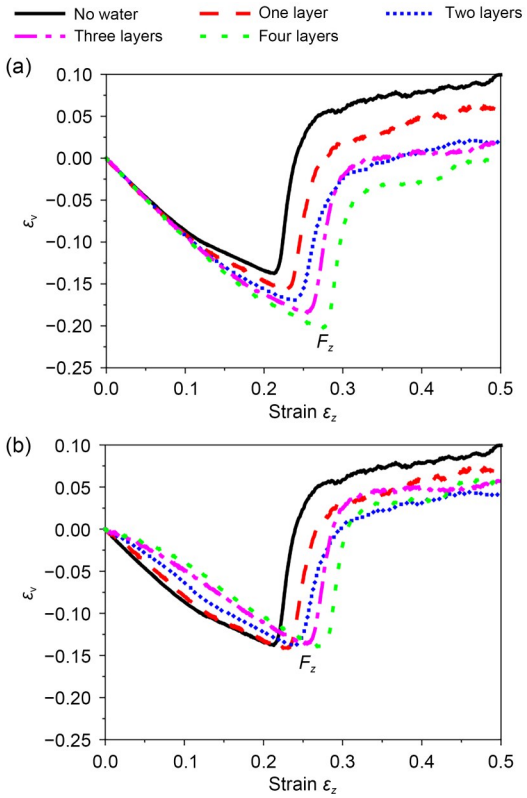

Fig. 6 Volumetric strain (ε_v) of clay–water system (a) and clay mineral sheets (b) when compressed along the *z*-direction

for all the clay mineral sheet cases are almost equal. Hence, the enhanced compressive deformation of the system is mainly due to the increase in the water film thickness. The water film helps guard against the failure of hydrated kaolinite.

In Fig. 6b, the failure volumetric strains (ε_v) of the five cases are almost equal, showing that the critical conditions for crushing clay mineral sheets are the same (e.g., the critical length when the covalent bond of the clay mineral sheet is crushed). Moreover, the failure strain (ε_z) increases as the water film thickness increases. Like in Fig. 6a, hydrated kaolinite is crushed more slowly thanks to the water film delaying the mutual extrusion of the two adjacent clay mineral sheets. Therefore, when hydrated kaolinite is compressed, the water film is compressed first, and the connections of the water film (i.e., non-bond and hydrogen bonds) are broken.

3.3 Failure mechanism

3.3.1 Stretching along the *x*-direction

In the ClayFF force field, the calculation of kaolinite's covalent bonds is included in the formula of the non-bond interactions (such as van der Waals forces and Coulomb potential energy, shown as Eqs. (S1) and (S2), respectively). Figs. S4 and S5 in the ESM thoroughly explain the analysis of non-bond interactions. Therefore, the bond-breaking phenomenon of kaolinite sheets can be understood by analyzing the interaction energy ($E_{\text{interaction}}$) of St···Ob, Ao···Ob, and Ao···Oh ($E_{\text{interaction}}=E_{\text{non-bond}}=E_{\text{van der Waals}}+E_{\text{electrostatic}}$), as shown in Fig. 7. The negative value indicates the interaction between two atoms. An increasing interaction energy means that the atomic bond is elongated. When the interaction energy changes suddenly, this is considered the breaking of a bond. The strain corresponding to the dashed line is the failure strain (ε_x=0.13).

By comparing the positions of the mutation point of three curves, one can see that the covalent bonds break in the order of Ao···Oh, St···Ob, and then Ao···Ob, which shows that the most easily broken bond is Ao···Oh (Duque-Redondo et al., 2014). Interestingly, the mutation point of Ao···Oh is very close to the position of the dashed line (failure strain). Thus, the structural failure of hydrated and dehydrated kaolinite should start with the breaking of the Ao···Oh bond (the critical value of its breaking is Δl_x≈8.09 Å, as mentioned in Fig. 5) and then lead to the dissolution of the other two covalent bonds.

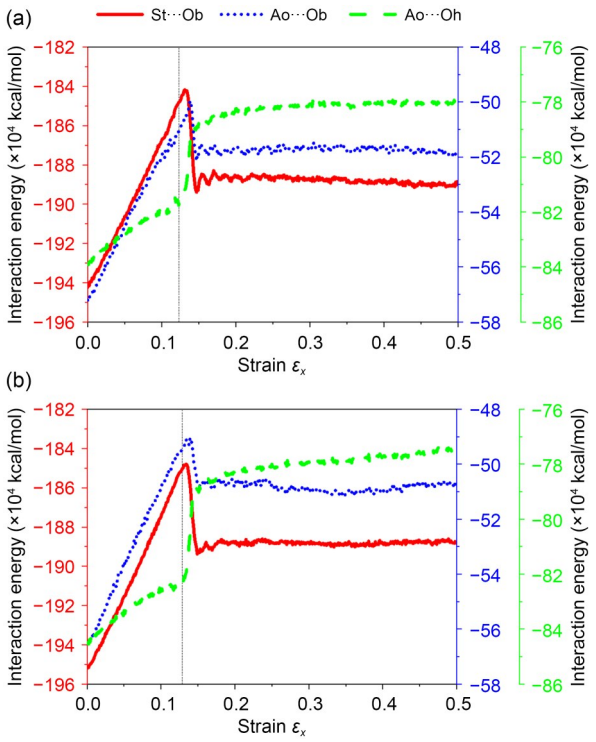

Fig. 7 Interaction energy of atomic pairs in clay mineral sheets when dehydrated (a) and hydrated (b) kaolinite are stretched along the *x*-direction. The hydrated kaolinite is the case with one layer of water film (1 kcal=4185.85 J)

Observing the interaction energy not only elucidates the order of bond breaking, but also showcases the law of bond rebounding. Different trends occurred after the mutation point was passed. For the St···Ob and Ao···Oh bonds, the interaction energy suddenly decreased after the mutation point, indicating a sudden shortening of the atomic distance. The reason for this is that at the moment when the St···Ob and Ao···Oh bonds break on the fracture surface, those on the non-fracture surface rebound. Conversely, the Ao···Ob curve shows an upward trend after the mutation point, meaning that the rebounding ability of the Ao···Oh bond is weak. Fig. 8 details the phenomenon of the fracture and rebound of three covalent bounds.

3.3.2 Compression along the *z*-direction

The changes in the van der Waals and Coulomb potential energy of the system during the compressive process are presented in Fig. 9. The van der Waals potential energy (red line), displaying a positive value, is mainly repulsive. Before failure, the atomic spacing becomes smaller under compression, leading to increased van der Waals repulsion. Then, the arrangement of atoms

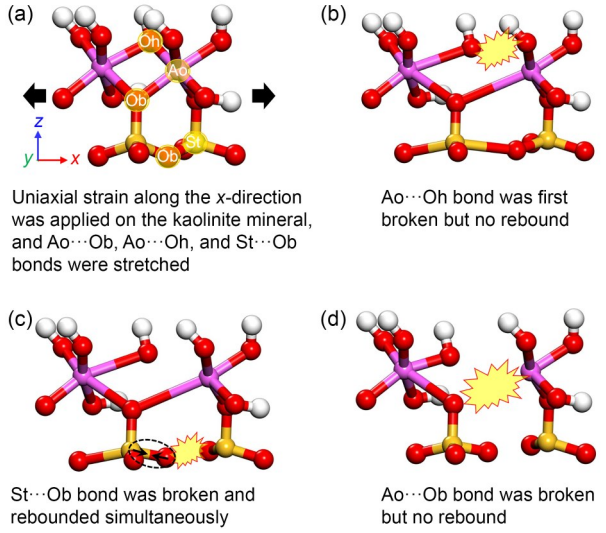

Fig. 8 Order (a–d) of the three kinds of bond breaking (Ao···Ob, Ao···Oh, and St···Ob) of clay mineral sheets in the tensile process (in *x*-*z* plane). The colors of the atoms are the same as in Fig. 1. References to color refer to the online version of this figure

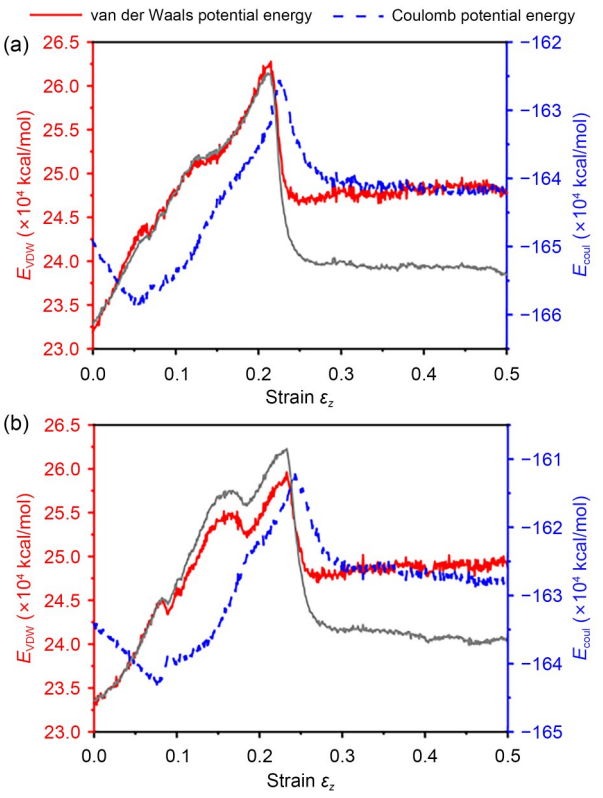

Fig. 9 Evolution of the van der Waals potential energy (E_{VDW}) and Coulomb potential energy (E_{coul}) of dehydrated (a) and hydrated (b) kaolinite in the compressive process. The hydrated kaolinite is the case with one layer of water film. The gray lines are the stress–strain curves for each case; see Fig. 3a for details. References to color refer to the online version of this figure

becomes disordered after failure, resulting in a decrease in the van der Waals force. Interestingly, the development of the van der Waals energy almost parallels the stress–strain curve (gray line), which shows that the van der Waals force determines the stress and failure with compressive deformation. The compressive stress increases with the van der Waals repulsion, and vice versa.

In contrast, the negative Coulomb interaction energy (blue line) shows that the attraction between atoms with opposite charges is more significant. As the atomic spacing is compressed, the increases in attraction and repulsion are not synchronized, resulting in complex changes in the Coulomb potential energy curve. For instance, the curve initially decreases (before approximately ε_z=0.1), indicating a more significant increase in Coulomb attraction. Moreover, the mutation point of the Coulomb potential energy lags behind the failure point F_z of the stress–strain curve.

The interaction energies of different components in the clay system were analyzed to understand the unique phenomenon of the Coulomb energy curve. The curves in Fig. 10a represent the interaction energies of clay–clay, clay–water, and water–water for the case of one water film layer. One can see that the interaction energy curves of the clay–clay and clay–water decreased before ε_z=0.1. Hence, the compression of clay–clay and clay–water is evident at this stage, which is the reason for the enhanced Coulomb attraction (Fig. 9b). In addition, the hysteresis of the mutation point of the clay–clay curve leads directly to that of the Coulomb potential energy (Fig. 9b). It is also worth mentioning that the interaction energy curve of water–water is continually increasing, and the calculated hydrogen bonding energy (Martin, 1960; Neder et al., 1999) is constantly decreasing (Fig. S7 of the ESM), indicating that the water film is becoming looser during the compression process.

In Fig. 10b, the interaction energy for the clay–clay case was divided into the energy between different clay mineral sheets, and the energy within the clay mineral sheets. Before ε_z=0.1 (Fig. S3 shows the enlarged image), the interaction energy of clay–clay (black line) decreased because of the decrease in interaction energy between different clay mineral sheets (red line). This stage is dominated by compression between different clay mineral sheets, which mainly manifests in the enhancement of the Coulombic attraction component of the interaction energy. When ε_z is in the range between

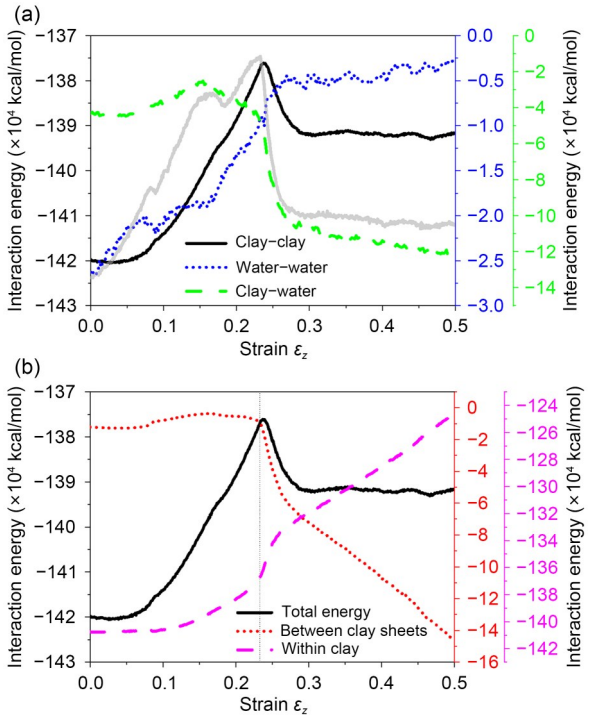

Fig. 10 Interaction energies between different components in kaolinite with one water film layer: (a) interaction energies of clay–clay, water–water, and clay–water; (b) the total interaction energy of clay–clay, the interaction energy between different clay mineral sheets, and that within clay mineral sheets. For comparison, the gray curve in Fig. 10a is the stress–strain curve of kaolinite with one water film layer in Fig. 3a

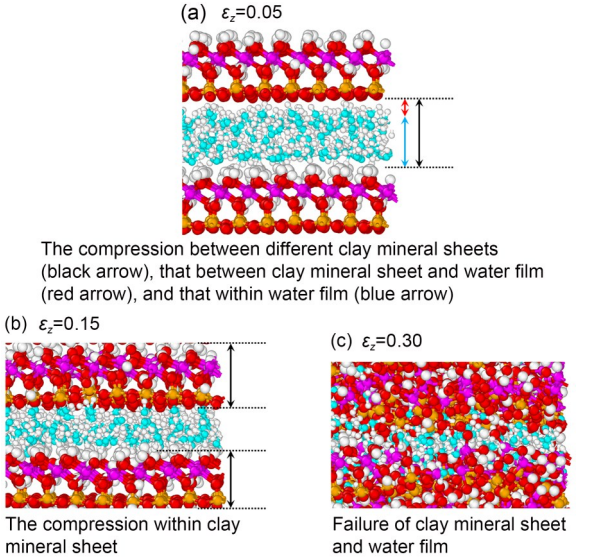

Fig. 11 Schematic diagram of clay mineral sheets and water films being compressed along the *z*-direction: (a) ε_z=0.05; (b) ε_z=0.15; (c) ε_z=0.30. References to color refer to the online version of this figure

0.10 and 0.23, the sharp increase of interaction energy within the clay mineral sheets (purple line) dominates the change of the clay–clay curve (black line). The compression at this stage mainly manifests in an enhanced van der Waals repulsion force as part of the interaction energy. In addition, because of the different changes in these two curves, the mutation point of the clay–clay curve lagged behind similarly to the Coulombic potential energy (in Fig. 9b).

The compressive process along the *z*-direction can be explained as follows. The first stage (before ε_z=0.1) is the compression of the water film itself, compression between the water film and the clay mineral sheet (the hydrogen bonds of clay···water increase at this stage, as shown in Fig. S4), and compression between different clay mineral sheets. The second stage (from ε_z=0.1 to the failure point) mainly involves intense compression within the clay mineral sheets. The third stage (after the failure point) is the crushing of the system and particularly the internal structure of the clay mineral sheets. Fig. 11 briefly illustrates the compressive process.

4 Conclusions

We investigated the influence of water films on the mechanical properties of kaolinite via MD simulation of uniaxial stretching and compression.

The water films significantly weakened the tensile and compressive properties of hydrated kaolinite. For one to four layers of water films, the tensile strength along the *x*-direction decreased by amounts ranging from 8.12% to 27.53%, and the compressive strength along the *z*-direction reduced by amounts ranging from 15.71% to 26.02%.

When stretched along the *x*-direction, the tensile strength of the hydrated kaolinite was weakened because of the unstable diffusion of water molecules. When compressed along the *z*-direction, the water film increased the volume of the hydrated kaolinite and accordingly weakened the compressive stress on the system.

The tensile failure along the *x*-direction was due to the breaking of covalent bonds in the kaolinite mineral sheet. Through analysis of the energy changes, we found that the bonds were broken in the order of Ao···Oh, St···Ob, and finally Ao···Ob.

The compressive failure and stress along the *z*-direction were dominated by the van der Waals repulsion between atoms. The overall compression process first involved compression of water–water, then water–clay

and clay–clay, and finally compression within the clay mineral sheets.

This study helps to explain the physical properties of hydrated kaolinite in high-stress environments, specifically the stress/strain, deformation, and the breaking of bonds, which may support resource extraction and disaster prevention and mitigation in extreme conditions. Moreover, further investigations can be made into chemical processes between clay and water, and their resulting impact on mechanical properties.

Acknowledgments

This work is supported by the National Natural Science Foundation of China (No. 52009149) and the Guangdong Basic and Applied Basic Research Foundation (No. 2021A1515012612), China.

Author contributions

Ming LU and Qiufeng DIAO designed the research, processed the corresponding data, and wrote the first draft of the manuscript. Yuanyuan ZHENG helped to organize the manuscript. Yuanyuan ZHENG and Ming LU revised and edited the final version.

Conflict of interest

Ming LU, Qiufeng DIAO, and Yuanyuan ZHENG declare that they have no conflict of interest.

References

Armand G, Noiret A, Zghondi J, et al., 2013. Short- and long-term behaviors of drifts in the Callovo-Oxfordian claystone at the Meuse/Haute-Marne Underground Research Laboratory. *Journal of Rock Mechanics and Geotechnical Engineering*, 5(3):221-230. https://doi.org/10.1016/j.jrmge.2013.05.005

Benco L, Tunega D, Hafner J, et al., 2001. Upper limit of the O–H···O hydrogen bond. Ab initio study of the kaolinite structure. *The Journal of Physical Chemistry B*, 105(44): 10812-10817. https://doi.org/10.1021/jp0124802

Chen J, Min FF, Liu LY, et al., 2019. Mechanism research on surface hydration of kaolinite, insights from DFT and MD simulations. *Applied Surface Science*, 476:6-15. https://doi.org/10.1016/j.apsusc.2019.01.081

Cygan RT, Liang JJ, Kalinichev AG, 2004. Molecular models of hydroxide, oxyhydroxide, and clay phases and the development of a general force field. *The Journal of Physical Chemistry B*, 108(4):1255-1266. https://doi.org/10.1021/jp0363287

Duque-Redondo E, Manzano H, Epelde-Elezcano N, et al., 2014. Molecular forces governing shear and tensile failure in clay-dye hybrid materials. *Chemistry of Materials*, 26(15):4338-4345. https://doi.org/10.1021/cm500661d

Fan QC, Wang ZP, Meng X, et al., 2022. Multi-scale analysis of the strengthening mechanism of functionalized graphene as reinforcement in cement composites. *Colloids and Surfaces A: Physicochemical and Engineering Aspects*, 651:129729. https://doi.org/10.1016/j.colsurfa.2022.129729

Fan QC, Zheng YY, Liu YM, et al., 2023. Effect of modified cellulose nanocrystals on the structure of calcium silicate hydrate studied by molecular dynamics simulation and experiment. *Langmuir*, 39(46):16244-16260. https://doi.org/10.1021/acs.langmuir.3c01601

Geng ZC, Tang SW, Wang Y, et al., 2024. Stress relaxation properties of calcium silicate hydrate: a molecular dynamics study. *Journal of Zhejiang University-SCIENCE A (Applied Physics & Engineering)*, 25(2):97-115. https://doi.org/10.1631/jzus.A2300476

González NA, Rouainia M, Arroyo M, et al., 2012. Analysis of tunnel excavation in London clay incorporating soil structure. *Géotechnique*, 62(12):1095-1109. https://doi.org/10.1680/geot.11.P.030

Hoover WG, 1985. Canonical dynamics: equilibrium phase-space distributions. *Physical Review A*, 31(3):1695-1697. https://doi.org/10.1103/PhysRevA.31.1695

Jorgensen WL, Chandrasekhar J, Madura JD, et al., 1983. Comparison of simple potential functions for simulating liquid water. *The Journal of Chemical Physics*, 79(2):926-935. https://doi.org/10.1063/1.445869

Kalinichev AG, Wang JW, Kirkpatrick RJ, 2007. Molecular dynamics modeling of the structure, dynamics and energetics of mineral-water interfaces: application to cement materials. *Cement and Concrete Research*, 37(3):337-347. https://doi.org/10.1016/j.cemconres.2006.07.004

Leng YS, Cummings PT, 2006. Hydration structure of water confined between mica surfaces. *The Journal of Chemical Physics*, 124(7):074711. https://doi.org/10.1063/1.2172589

Liu XD, Lu XC, Wang RC, et al., 2012. Atomic scale structures of interfaces between kaolinite edges and water. *Geochimica et Cosmochimica Acta*, 92:233-242. https://doi.org/10.1016/j.gca.2012.06.008

Lu M, Diao QF, Zheng YY, et al., 2024a. Influence of water on tensile behavior of Illite through the molecular dynamics method. *International Journal of Geomechanics*, 24(4): 04024024. https://doi.org/10.1061/IJGNAI.GMENG-8999

Lu M, Huang W, Zheng YY, 2024b. Molecular dynamics simulation study of the effects of water content and wettability on the shear properties of kaolinite for the failure of clay soil. *ACS Applied Nano Materials*, 7(3):2843-2854. https://doi.org/10.1021/acsanm.3c05023

Lu M, Zheng YY, Yin ZY, 2024c. From sedimentation to consolidation of kaolinite: a molecular dynamic study. *Computers and Geotechnics*, 170:106285. https://doi.org/10.1016/j.compgeo.2024.106285

Lu M, Zheng YY, Yin ZY, 2025. Investigating the consolidation of kaolinite with molecular dynamics: the micro effective stress principle. *Applied Surface Science*, 690: 162653. https://doi.org/10.1016/j.apsusc.2025.162653

Ma ZY, Pathegama Gamage R, Rathnaweera T, et al., 2019.

Review of application of molecular dynamic simulations in geological high-level radioactive waste disposal. *Applied Clay Science*, 168:436-449. https://doi.org/10.1016/j.clay.2018.11.018

Martin RT, 1960. Adsorbed water on clay: a review. *Clays and Clay Minerals (National Conference on Clays and Clay Minerals)*, 9:28-70. https://doi.org/10.1346/CCMN.1960.0090104

Milheiro FAC, Freire MN, Silva AGP, et al., 2005. Densification behaviour of a red firing Brazilian kaolinitic clay. *Ceramics International*, 31(5):757-763. https://doi.org/10.1016/j.ceramint.2004.08.010

Moreno-Maroto JM, Alonso-Azcárate J, 2015. An accurate, quick and simple method to determine the plastic limit and consistency changes in all types of clay and soil: the thread bending test. *Applied Clay Science*, 114:497-508. https://doi.org/10.1016/j.clay.2015.06.037

Neder RB, Burghammer M, Grasl T, et al., 1999. Refinement of the kaolinite structure from single-crystal synchrotron data. *Clays and Clay Minerals*, 47(4):487-494. https://doi.org/10.1346/CCMN.1999.0470411

Plimpton S, 1995. Fast parallel algorithms for short-range molecular dynamics. *Journal of Computational Physics*, 117(1): 1-19. https://doi.org/10.1006/jcph.1995.1039

Porion P, Michot LJ, Faugère AM, et al., 2007. Structural and dynamical properties of the water molecules confined in dense clay sediments: a study combining ^{2}H NMR spectroscopy and multiscale numerical modeling. *The Journal of Physical Chemistry C*, 111(14):5441-5453. https://doi.org/10.1021/jp067907p

Pouvreau M, Greathouse JA, Cygan RT, et al., 2019. Structure of hydrated kaolinite edge surfaces: DFT results and further development of the ClayFF classical force field with metal–O–H angle bending terms. *The Journal of Physical Chemistry C*, 123(18):11628-11638. https://doi.org/10.1021/acs.jpcc.9b00514

Smirnov KS, Bougeard D, 1999. A molecular dynamics study of structure and short-time dynamics of water in kaolinite. *The Journal of Physical Chemistry B*, 103(25):5266-5273. https://doi.org/10.1021/jp9900281

Šolc R, Gerzabek MH, Lischka H, et al., 2011. Wettability of kaolinite (001) surfaces—molecular dynamic study. *Geoderma*, 169:47-54. https://doi.org/10.1016/j.geoderma.2011.02.004

Spagnoli G, Sridharan A, Oreste P, et al., 2017. A probabilistic approach for the assessment of the influence of the dielectric constant of pore fluids on the liquid limit of smectite and kaolinite. *Applied Clay Science*, 145:37-43. https://doi.org/10.1016/j.clay.2017.05.009

Sun HM, Yang W, Chen RP, et al., 2021. Microfabric characteristics of kaolinite flocculates and aggregates—insights from large-scale molecular dynamics simulations. *Applied Clay Science*, 206:106073. https://doi.org/10.1016/j.clay.2021.106073

Suter JL, Coveney PV, Greenwell HC, et al., 2007. Large-scale molecular dynamics study of montmorillonite clay: emergence of undulatory fluctuations and determination of material properties. *The Journal of Physical Chemistry C*, 111(23):8248-8259. https://doi.org/10.1021/jp070294b

Tang SW, A HB, Chen JT, et al., 2019. The interactions between water molecules and C-S-H surfaces in loads-induced nanopores: a molecular dynamics study. *Applied Surface Science*, 496:143744. https://doi.org/10.1016/j.apsusc.2019.143744

Tararushkin EV, Pisarev VV, Kalinichev AG, 2022. Atomistic simulations of ettringite and its aqueous interfaces: structure and properties revisited with the modified ClayFF force field. *Cement and Concrete Research*, 156:106759. https://doi.org/10.1016/j.cemconres.2022.106759

Tunega D, Gerzabek MH, Lischka H, 2004. Ab initio molecular dynamics study of a monomolecular water layer on octahedral and tetrahedral kaolinite surfaces. *The Journal of Physical Chemistry B*, 108(19):5930-5936. https://doi.org/10.1021/jp037121g

Wei PC, Zheng YY, Zaoui A, et al., 2023. Atomistic study on thermo-mechanical behavior and structural anisotropy of montmorillonite under triaxial tension and compression. *Applied Clay Science*, 233:106817. https://doi.org/10.1016/j.clay.2023.106817

Wongsaroj J, Soga K, Mair RJ, 2013. Tunnelling-induced consolidation settlements in London clay. *Géotechnique*, 63(13): 1103-1115. https://doi.org/10.1680/geot.12.P.126

Yang H, He MC, Lu CS, et al., 2019. Deformation and failure processes of kaolinite under tension: insights from molecular dynamics simulations. *Science China Physics, Mechanics & Astronomy*, 62(6):64612. https://doi.org/10.1007/s11433-018-9316-3

Zhang CL, 2018. Thermo-hydro-mechanical behavior of clay rock for deep geological disposal of high-level radioactive waste. *Journal of Rock Mechanics and Geotechnical Engineering*, 10(5):992-1008. https://doi.org/10.1016/j.jrmge.2018.03.006

Zhang LH, Lu XC, Liu XD, et al., 2014. Hydration and mobility of interlayer ions of (Na_x, Ca_y)-montmorillonite: a molecular dynamics study. *The Journal of Physical Chemistry C*, 118(51):29811-29821. https://doi.org/10.1021/jp508427c

Zhang LL, Zheng YY, Wei PC, et al., 2021. Nanoscale mechanical behavior of kaolinite under uniaxial strain conditions. *Applied Clay Science*, 201:105961. https://doi.org/10.1016/j.clay.2020.105961

Zhang Z, Song XY, 2022. Molecular dynamics modeling of cracks in dry clay sheets at the nanoscale. *Computers and Geotechnics*, 152:105037. https://doi.org/10.1016/j.compgeo.2022.105037

Zhao MH, Zou XJ, Zou PX, 2007. Disintegration characteristics of red sandstone and its filling methods for highway roadbed and embankment. *Journal of Materials in Civil Engineering*, 19(5):404-410. https://doi.org/10.1061/(ASCE)0899-1561(2007)19:5(404)

Electronic supplementary materials

Eqs. (S1)–(S6), Figs. S1–S7, Table S1